PERGAMON

Journal of Structural Geology 22 (2000) 1285–1296

JOURNAL OF STRUCTURAL GEOLOGY

www.elsevier.nl/locate/jstrugeo

A model of displacement and strain for arc-shaped mountain belts applied to the Jura arc

David Hindle[a,*,1], Olivier Besson[b], Martin Burkhard[a]

[a]*Institut de Géologie, rue E. Argand 11, CP 2, CH 2007 Neuchâtel, Switzerland*
[b]*Institut de Mathématiques, rue E. Argand 11, CP 2, CH 2007 Neuchâtel, Switzerland*

Received 15 July 1999; accepted 9 March 2000

Abstract

A plan view geometric model for simple, parallel, differential displacements is presented. As an analogue for models of arcuate mountain belt formation we use the model to predict strain patterns produced by parallel displacement in front of a rigid versus deformable indenter. A rigid indenter is simulated by an irregular quadrilateral displaced a constant amount along its hinterland boundary. A deformable indenter is simulated by an irregular quadrilateral displaced along a hinterland boundary that is allowed to rotate. Some simple test cases show that the deformable indenter model leads to a pattern of strain very similar to that encountered in arcuate mountain belts. Short axes orientations are most deviated from the transport direction along the lateral edges of the model with minimum displacement and shortening and vary across the central domain, mirroring strain features with variable orientations from mountain belts such as fold trends and minor deformation features such as horizontal stylolite peaks. The rigid indenter model also generates short axes deviated from the transport direction but showing far less variation. Displacement–strain relationships from the Jura mountains (Switzerland and France) are quantified based upon a simplified version of the finite displacement field for the Jura fold–thrust belt of Philippe, Y. (1995) [''Rampes latérales et zones de transfer dans le chaines plissées''. (Unpublished PhD thesis, Université de Savoie)]. We find that the model short axis orientation pattern is very similar over at least the eastern and central Jura to the stylolite patterns from the region whilst the long axes closely match the fold axes trends. The model suggests that the Jura mountains could have formed as a result of a progressive deformation with uniform transport in a general northwest direction.

1. Introduction

The form of arcuate fold and thrust belts has long fascinated geologists (Argand, 1922; Carey, 1955; Ries and Shackleton, 1976; Marshak, 1988; Ferrill and Groshong, 1993). Intuitive interpretations of a curved mountain belt suggest the need for radial movement of material to produce the curved fold axis patterns we witness (Argand, 1922; Carey, 1955). Radial displacement of any form will immediately create a space problem for the material in the arc which will have to 'stretch' drastically to accommodate the movement (Ferrill and Groshong, 1993). Restoring such a system could lead to all material moving back to a single point—a source-sink. Evidence for the large strike parallel extensions required by such a mechanism is lacking. More careful consideration of the problem has led to the conclusion that material constrained to move in a uniform direction can create strongly curved fold patterns (Ries and Shackleton, 1976; Ferrill and Groshong, 1993). Such differential shear models have, up until now, focused on distinguishing fold–thrust belt curvature forming mechanisms. These studies particularly emphasised the importance of the pattern of tangential elongation as the key parameter for dis-

* Corresponding author. Tel.: +49-331-288-1313; fax: +49-331-288-1370.
E-mail address: hindle@gfz-potsdam.de (D. Hindle).
[1] Now at: GeoForschungsZentrum Potsdam, Projektbereich 3.1 Telegrafenberg C223, D-14473 Potsdam, Germany

0191-8141/00/$ - see front matter
PII: S0191-8141(00)00038-9

tinguishing between curve forming mechanisms (e.g. transport parallel simple shear, radial thrusting, pure bending, etc.). There has also been some confusion over what are the possible arc geometries resulting from different variants of differential shear. Displacement–strain relationships have sometimes been drawn intuitively, and incorrectly. For instance, both Ries and Shackleton (1976) and Marshak (1988) suggested that uniformly shortened regions with boundaries that are not orthogonal to transport direction would have fold axes orthogonal to the transport direction. This is shown (see Fig. 2, model 1) to be untrue. Often relationships between displacement and strain are counter-intuitive, and only a mathematical derivation of the strain pattern from the displacement field is sure to give correct results. This is an extension of the relationship between displacement and strain of which geologists have long been aware (Howard, 1968; Means, 1976; Ramsay, 1976).

If we accept differential shear as a mechanism for arc formation, two model classes can be distinguished based on what happens not in the thrust belt itself, but in the region indenting it. These follow from the work of Hindle and Burkhard (1999) which clarifies the fundamental differences between many proposed arc formation models. We only produce models of the 'Primary arc' type defined by Hindle and Burkhard (1999) and give more precise numerical data on the effects of deformation and its relationship to different displacement geometries. The aim is to try and identify which model is the most plausible for forming arcs. Therefore, we demonstrate the rationale of displacement–strain models for very simple, geometric analogues to arcuate fold and thrust belts and then compare these models to a real example: the Jura arc, part of the western alpine collisional system.

The Jura mountains are the latest (Middle Miocene onward) and most external part of the northwestern alpine deformation zone (Sommaruga, 1999). They are a small (ca. 350 km long) arcuate (the trend of the mountains varies by 90° along their length), fold and thrust belt, varying in width from 0 km at the eastern end to around 65 km in their central portion. They have been interpreted as being both a thick-skinned fold and thrust belt with various basement structures thought to be involved in their evolution [e.g. wrench faulting in the basement folding the cover above (Pavoni, 1961), penetration of basement thrusts into the cover (Aubert, 1945), crustal delamination due to a shallow dipping basement thrust soling out in the crust (Ziegler, 1982)] or a thin-skinned, allochthonous belt, with the Mesozoic cover shortened above an evaporite detachment regionally present within the Triassic (Schardt, 1906; Schardt, 1908; Buxtorf, 1916; Burkhard, 1990; Sommaruga, 1995; Burkhard and Sommaruga, 1998; Sommaruga, 1999). Most recently, these ideas have been based on regional interpretation of industry seismic lines across the Swiss Molasse Basin and Jura which are now publicly available. When combined with balancing arguments, the autochthonous, thin-skinned interpretation for the Jura mountains is the most reasonable. We base all our modelling on a thin-skinned interpretation. The results of our modelling show that the fold axes trends and orientation of horizontal stylolite peaks (regional strain markers for the Jura) can be simulated by the long and short axes produced by a model of differential shortening with uniform transport direction.

2. A simple, geometric, displacement–strain model

2.1. Model characteristics

In order to show the effect of displacement of material seen in plan view on the strain pattern within that material we adopt a geometric approach. Mechanical properties of rocks are considered isotropic and homogeneous. A starting point for a model is a quadrilateral. This geometry was used before by Ferrill and Groshong (1993) describing the parallel displacement of material across the length of arcuate fold belts.

With suitable mathematical manipulation (see Appendix A), we can use any quadrilateral form we

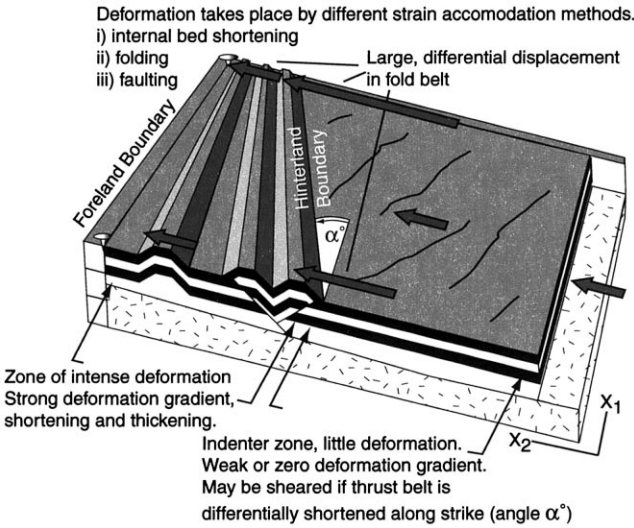

Fig. 1. A hypothetical fold and thrust belt illustrating the idea of a displacement gradient. In the picture above, there are gradients in the transport direction, which is considered to be unique, and also along strike of the mountain belt, since there is a differential displacement in this direction. The diagram makes a clear separation between an indenter region undergoing passive transport but also lightly deformed by shearing, pushing into a mountain belt which is strongly differentially shortened along strike and which deforms by thrusting and folding. Displacement drops to zero across the width of the fold belt (shown by 'pins') creating a displacement gradient orthogonal in the X_2 direction.

wish. However, to create a parallel displacement field, the corners must move in a parallel direction. The behaviour of an indenting region to an arcuate fold and thrust belt is also of considerable interest in these problems. The indenter and thrust belt are joined to each other (see Fig. 1), and any movement of their common boundary must also be present in the indenting region. Consequently, if the common boundary twists or rotates, this component of movement will be present in the indenter too, and should be reflected in the deformation pattern found there. If there is no twist or rotation, but simply a constant translation of the boundary, it is possible that the indenter will behave as a rigid block and show very little deformation. Burkhard (1990) discussed some of the different possible arc-indenter configurations in the context

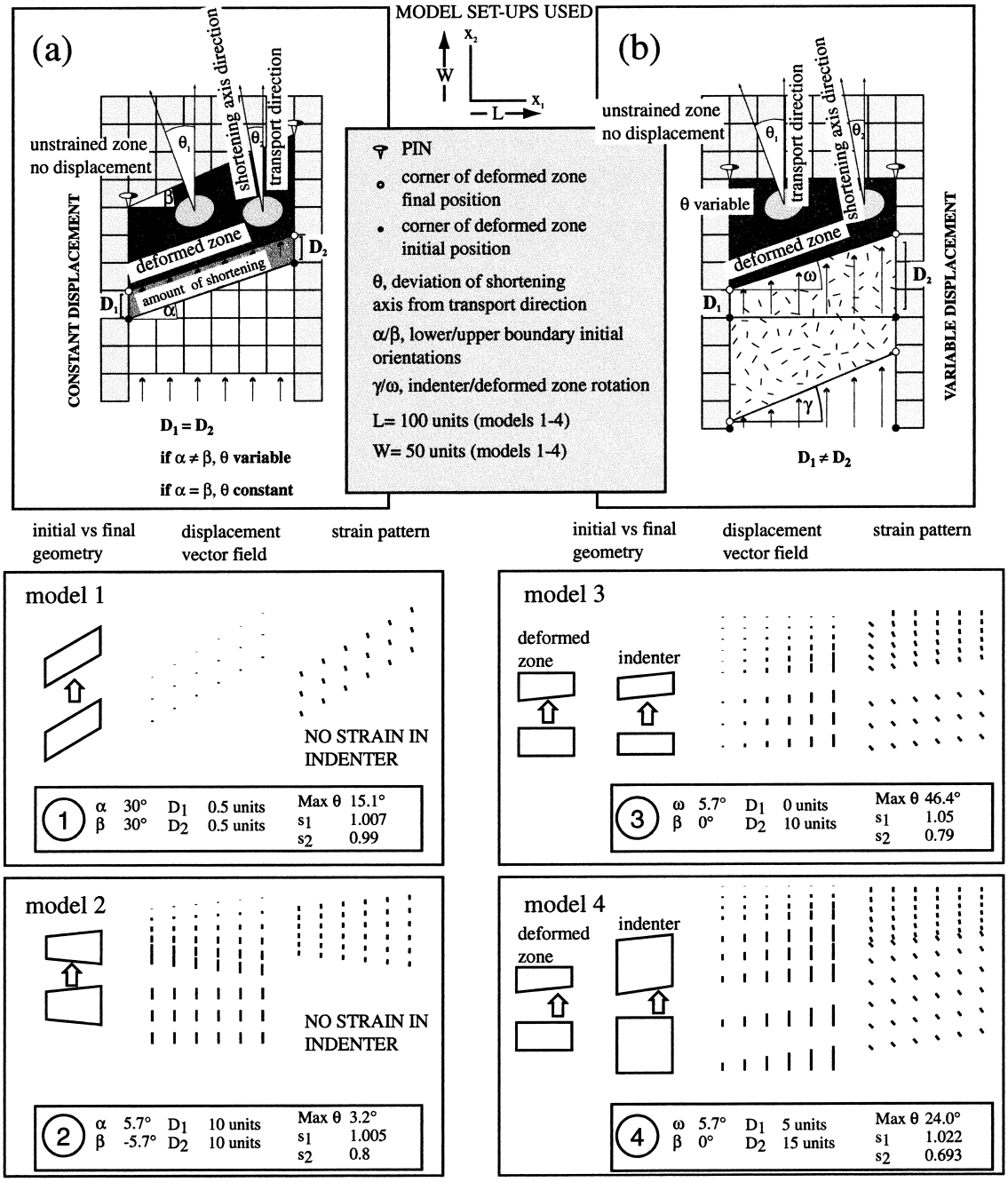

Fig. 2. Illustrative models for deformation patterns generated by transport parallel simple shear. Two types of model are used, (a) shows a 'rigid indenter' and (b) shows a deformed indenter. Model results numbered 1–4 are presented which show graphical plots of both displacement vectors and shortening axes (in their correct orientation) shown to scale and summarise the boundary conditions (α, β, γ, ω, D) and the resulting maximum values of shortening and lengthening (s_3 and s_1) and maximum angle (θ) between s_3 and the transport direction in smaller numbered boxes.

of the Jura arc and identified four models for the indenter, all variants of deformed or undeformed indenters. These broad categories provide useful boundary conditions for the models. A rigid indenter neatly translates into constant displacement of material along the thrust belt/indenter limit, whilst a deformable indenter allows variable displacement along this boundary. We apply the additional constraint of material always moving parallel, and produce four illustrative models, two with an 'undeformed indenter', two with a 'deformed indenter'.

The rigid indenter models (Fig. 2a, and models 1 and 2) have deformed zone boundaries which are oblique to the transport direction of the rigid indenter. The common indenter/deformed zone boundary moves by a constant amount along its width ($D_1 = D_2$). The same movement distance is applied to every point in the indenter, which undergoes a rigid body translation. Within the deformed zone, the displacement decreases smoothly to zero by the foreland edge of the deformed zone, generating a displacement gradient in the direction of transport. The models vary by changing the inclinations of the foreland and indenter/fold belt boundaries, producing homogeneous ($\alpha = \beta$) or inhomogeneous ($\alpha \neq \beta$) deformation.

Such models were seen as analogous to arc forming mechanisms by many authors (Carey, 1955; Ries and Shackleton, 1976; Marshak, 1988). They are a direct analogue to model B of Burkhard (1990), for the Molasse–Jura system where a rigid Molasse Basin pushes east–west, obliquely into the Jura mountains.

The deformable indenter models (Fig. 2b) have a deformed region/indenter common boundary undergoing a rotation (angle ω), which also affects material in the indenter region. The indenting region may have a hinterland boundary undergoing a different rotation (γ). The indenter region is deformed as a result. The 'thrust belt' itself will be inhomogeneously deformed as the model is set up with a fixed foreland boundary and a rotated boundary common with the indenter. The two models presented have similar characteristics to the transport parallel simple shear idea of Ferrill and Groshong (1993).

2.2. Mathematical principle

The quantity known as the displacement gradient is the key to the following models. Displacement gradient refers to changes in the total displacement of points between the original state and the deformed state along a particular direction. Hence, we could define such a quantity along only one coordinate axis, and have effectively a one-dimensional quantity, or we could envisage it existing in all directions in a plane, and have a fully two-dimensional quantity, shown conceptually in Fig. 1. The idea is thoroughly dealt with by Means (1976).

In our analysis of fold–thrust belt curvature formation, we make a distinction between the indenter zone and the fold–thrust belt itself (Fig. 1). The two regions are joined and continuous but there is a jump in the displacement gradient between them. The displacement vectors in the thrust belt diminish in magnitude in the transport direction, reaching zero along the outer boundary of the thrust belt. There is a consequential horizontal shortening (and would be a vertical thickening) of the crust to accommodate the differential movement, which occurs through folding and faulting. The indenter undergoes the full movement of the most translated part of the fold–thrust belt, but all parts of the indenter move (approximately) the same distance in the transport direction at least, and hence the displacement gradient and consequently deformation, is very small.

A gradient orthogonal to the transport direction may also develop, resulting in transport parallel differential displacement (or what one may term differential shear). As the fold–thrust belt is pinned (see Fig. 1) along an arbitrary foreland boundary, all displacement of material reaches zero along this line. If any point of the indenter region moves further into the fold–thrust belt than adjacent points, there is a differential shortening in the fold–thrust belt itself according to the position in a direction orthogonal to material transport vectors for the thrust belt. This can be seen in Fig. 1, where displacement vectors have different lengths along this direction. The consequence of transport parallel differential displacement is a transport parallel, differential shear which produces a variable strain pattern in the region. We note (see Fig. 1) that in many thin-skinned mountain belts, horizontal movement of material is often more than an order of magnitude greater than vertical. In this paper we think particularly of the Jura arc, where horizontal shortening of 25–30 km is likely whilst relief due to thrusting is restricted to 1–2 km. Hence we can justify modelling displacement and strain in the horizontal plane only (i.e. in map view) and the problem reduces to two dimensions.

The displacement gradient can be described by a coordinate transformation matrix from which we derive the finite-strain tensor for the region. In a simple quadrilateral for instance, there is a relationship between the displacement gradient matrix $\mathbf{F}$, and the components of the individual displacement vectors affecting each of the quadrilateral corner points $\mathbf{P}_n$ (n = 1–4) which is demonstrated fully in the Appendix A. If we calculate this, we have a simple model for plan view strain. We use a quadrilateral domain since this evaluates a continuous function for strain across

its domain, equivalent to 'averaging' the displacement field due to folding, faulting, etc.

3. Model results

We have used four general models, two for undeformed indenters, and two for deformed indenters. They all have uniquely parallel material displacement vectors (assumed to be parallel to the X_2 axis of a general, Cartesian co-ordinate system) and yet all have short axes which are deviated from the transport direction. The degree of deviation varies according to the boundary conditions used. However, any model with a rotational boundary (indenter/fold belt common boundary) generally shows the strongest variability of orientation of short axes. In all models including those with constant boundary displacements we find differential displacements are generated along any line parallel to the X_1 axis and there are displacement gradients in all directions in the model plane. This occurs in spite of the uniquely parallel movement of material. The general model characteristics and specific results are laid out in Fig. 2.

3.1. Model 1

Model 1 involves constant displacement applied to a region of uniform width which is oblique to transport direction. It is a case previously considered by Sanderson and Marchini (1984). He recognised that even though shortening across a region is constant, if the transport is oblique to the region and even if it has a 'symmetrical' geometry (parallelogram) a differential displacement is generated. The result is a uniform directed θ (homogeneous deformation) differing from the transport direction (15°). The angle θ will vary as a function of both the obliquity of a region to transport and the amount of shortening.

3.2. Model 2

In model 2, a rigid indenter pushes into a zone of variable width and geometry, with both boundaries inclined to the transport direction ($\alpha = -5.7°$, $\beta = 5.7°$ measured from X_1). The resulting deformation is symmetric about the median line of the deformed zone, and is inhomogeneous. There are only tiny variations in the angle θ. The largest difference between the short axis and the X_2 axis is 3.2°. In the direction of maximum stretch, there is hardly any lengthening ($s_1 = 1.005$ maximum). This small difference in orientation of shortening axes reflects the very weak differential displacement along strike in the model.

3.3. Model 3

In model 3, we represent a deformable indenter, since the common indenter/deformed zone boundary undergoes rotation. This is a composite model of an arc and its indenter. The deformed zone is initially rectangular in shape, the common indenter/deformed zone boundary undergoing a zero displacement at its left extremity, and a maximum displacement at its right extremity (rotation, $\omega = 5.7°$). This produces an inhomogeneous deformation in the deformed zone, as there is no movement of the foreland boundary. To accommodate the movement, the indenter behind the deformed zone must also be sheared. In this case, both a homogeneous simple shear and shortening is applied to the indenter, which undergoes a small shortening and an equal rotation (= simple shear) of its foreland and hinterland boundaries. Deviations of shortening axes from the X_2 direction are far greater with this configuration. Maximum deviation occurs along the left-hand (unshortened) edge, where the state of strain is simple shear only. The remainder of the deformed zone is increasingly shortened resulting in lower angular deviations. A surprising consequence of this model is the 0° deviation of shortening axes along the upper boundary where the state of strain is pure shear only. This implies an instantaneous passage at some point from $\theta > 45$–0°. Assuming fold axes perpendicular to the local direction of s_3, the model would produce a series of curved folds becoming progressively more parallel to X_1 in the positive X_1 direction (similarly along X_2). There is also considerably more (up to 1.05) extension in the direction of the long axis.

3.4. Model 4

Model 4 contains the following important features. The deformed zone is shortened by a translational component of the common indenter/deformed zone boundary, in addition to a differential displacement of this boundary along strike. The indenter region also undergoes a differential shortening along strike. It is sheared to accommodate the displacements in the deformed zone, however, its hinterland boundary rotates more than its foreland boundary, creating differential shear ($\gamma = 8.5°$). Moreover, a small shortening component is applied to the whole zone (less than that applied to the deformed zone). Every point in the indenter has an additional translation applied to it. The translation is of the same amount as the additional shortening applied to the deformed zone. The indenter thus configured has a strain pattern with the deviation of shortening axes from X_2 decreasing in both positive X_1 and X_2 senses. The result of additional shortening in the fold-belt region of the model is to reduce the deviation of shortening axes from the

X_2 direction (compare to results for model 3 for instance).

4. Discussion

The model results demonstrate how differential shear in a deformed region leads to strains which are highly variable in both orientation (θ) and magnitude (stretches, s_1—maximum extension and s_2—maximum shortening). Differential shear is generated by both uniform displacement of the lower boundary to an irregularly shaped region or by rotation of a lower boundary of a regular or irregular region. Rotations cause large differential shear and consequently larger maximum θ and s_1/s_2. Any general, additional shortening across the region ($D_1 > 0$), leads to a reduction in maximum θ (see difference between models 2 and 3).

The geometries shown are scale independent and analogous to many geological situations. In arcuate mountain belts, we may examine the relationship between fold-axis orientations and other finite-strain markers such as stylolites or calcite twins, and transport direction of material in the region. We may assume predicted θ to be locally parallel to stylolite teeth and at 90° to fold axes. The conclusion would be that a configuration such as model 2 would resemble an arcuate mountain belt in many ways. However, this is slightly unrealistic since in a mountain belt, at such high strains, a large amount of displacement is taken up by faulting.

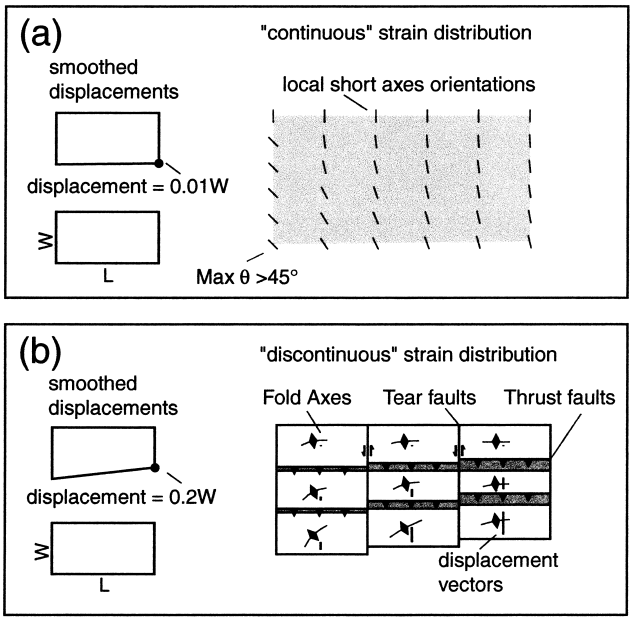

Fig. 3. Finite strain accumulates in small increments but the geometry of each increment may remain relatively constant over time. Small deformation features form from the onset of deformation whilst large-scale ones (faults and folds) form after many increments. (a) shows a tiny increment of transport parallel differential shear. The resulting fanning strain pattern has $\theta > 45°$ along one lateral edge of the model and $\theta \approx 0°$ along the opposite edge. Early strain features like stylolites should exhibit this sort of strain pattern too. (b) shows a larger amount of transport parallel differential shear, which could be thought of as resulting from 200 increments of (a). Deformation mechanisms change to accommodate the larger strain (shown schematically). Once faulting has begun, most new deformation will accumulate on faults, and the system will behave as a series of differentially translated, semi-rigid blocks. However, earlier-formed, low-deformation features would be present within these blocks and may preserve their original orientations.

Indeed, all the deformation accumulated by different mechanisms in a thin-skinned thrust belt can be thought of as accommodating some regional scale strain. The important thing to remember is the progressive nature of the deformation. Features such as stylolites and possibly some heterogeneities provoking early folding would begin forming in the very earliest stages of deformation of a region (Fig. 3a) when total strain is very low. This initial geometry of deformation may still be similar to that seen at the end of the episode. Indeed, the total finite deformation for transport parallel simple shear could be thought of as accumulating by a succession of increments such as in Fig. 3(a). Taking a similar rectangular domain as we have used for our first strain models, we apply a tiny displacement to one of its corners (Fig. 3a) and simulate one such increment. We see that even the smallest differential shear will give $\theta > 45°$. If this is the deformation geometry affecting an arcuate mountain belt, we would expect early strain features such as stylolites to form with orientations similar to predicted θ. Some early folding (and possibly faulting) could also be initiated in the same orientation. Further deformation (Fig. 3b) would be accommodated by faulting and folding, and may occur by translation of discrete, semi-rigid blocks. However, already formed folds and stylolites would keep their early orientations, which might be rotated passively if the differential shear continues.

Therefore, though the detailed processes governing formation of strain features are complicated, the orientations and patterns we find should be related to the geometry of deformation applied. Our modelling simulates the average or total strain applied to a region which may be accommodated by a number of mechanisms. Reches (1978) also suggested that groups of faults act together to accommodate regional strains and their orientation would have a clear relationship to the regional scale strain field that was developing. Even for simple homogeneous strains, four differently oriented fault planes would exist. Molnar (1983) suggested an inverse process where earthquake magnitudes on differently oriented faults could be summed to give an average regional strain. Both point to the fact that faults (and folds and intergranular defor-

mation) are allowing change of shape of a large region. We argue that at the scale of a whole mountain belt, an overall deformation geometry exists and this is the key to the regional strain pattern we find.

5. The Jura Arc example

Taking these arguments further requires a real example. The Jura fold-and-thrust belt is an arcuate region of more than 350 km lateral extent, lying northwest of the northern alpine foreland basin (Swiss Molasse). The belt is composed of thrust Mesozoic strata detached from a Permo-Carboniferous 'basement' by Triassic evaporite layers. Lateral thickness variations and pinch-outs of the Triassic 'Muschelkalk' and 'Keuper' series are a major control on displacement and shortening of the cover sequence over the width of the chain and its arcuate form (Debrand Passard et al., 1984; Philippe, 1994). Following Sommaruga (1996), the mechanical behaviour of the Jura strata can be broadly characterised as follows (see Fig. 4): limestone-dominated lithologies are generally strong and brittle; shale- and marl-dominated lithologies are weaker and may be either plastic or brittle according to associated temperature, fluid pressure and relative amount and type of clay; evaporite-dominated lithologies are weak, and generally plastic. Hence, the lowermost, salt-gypsum-dominated Triassic units of the Jura are mechanically by far the weakest, and form the principal basal décollement, whilst the Upper Malm, a thick, limestone unit is by contrast very strong and has deformed under a brittle regime across much of the belt to produce the fold–thrust system we see today. The Jura mountains contain remnants of the Tertiary foreland basin Molasse sequence proving that the foreland basin's foredeep unconformity

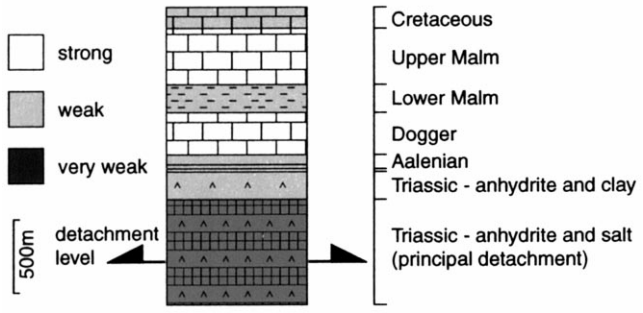

Fig. 4. Mechanical stratigraphy for the Jura mountains, adapted from Sommaruga (1996). Thicknesses shown are correct for the central Jura mountains, but vary across the chain as described in the text. The main décollement layer is illustrated by thrust arrows, and the approximate relative strengths of the lithologies are shown according to the shading of the units.

extended into the chain before it was formed. In the alpine foreland basin, hinterland to the Jura, the same Mesozoic layers dip below Molasse sediments up to 3 km thick at the alpine front. The entire wedge of Molasse and Mesozoic material remains relatively undeformed. Contractional deformation of the Mesozoic sequences in the Jura mountains develops from the post-Middle Miocene (Serravallian), onwards (Burkhard and Sommaruga, 1998).

Previous models of curvature formation in the Jura belt can be summarised according to two types of approach used. The first are based on two-dimensional, plan view restorations of the Jura (or parts of it). Hence, Laubscher (1961) originally formulated a model involving rotation of the Molasse/Jura limit, by 7° in the eastern part of the Jura mountains, constrained by the variations in shortening estimated along the strike of the belt from two-dimensional restoration. This model implies that the Jura mountains are then indented by a Molasse region which would also have been sheared. More recently, Philippe (1995) produced the most complete two-dimensional restoration of the Jura belt yet. The displacement field he derived relative to a pin line in the stable European foreland to the Jura shows an explicit rotation of the Jura/Molasse boundary, which could also mean that the Molasse Basin is a deformed (sheared) indenter. The second group of interpretations are based on static models for stress patterns suggested by different strain features found in the present-day Jura belt. Laubscher (1972) for instance, suggested a conceptually different model for curvature formation where the indenting block was effectively the western Alps (Helvetic and Prealpine nappes) pushing as a rigid block into the Molasse and Jura (i.e. both are indented but only the Jura shows significant deformation). This interpretation was chosen because the (instantaneous) stress pattern generated by such a rigid block pushing into a deformable hinterland would resemble a pattern of stress trajectories related to the variable orientation of the fold axes across the belt. Homberg et al. (1999) have recently proposed a modified indenter model in which the Molasse Basin is the direct indenter to the Jura arc; furthermore, Homberg proposes that this indenter would have broadened over time. The broadening is used as an explanation for two differing orientations of stress axes determined from sets of Mio-Pliocene fault slickenslides which pre- or post-date folding in the Jura.

The difference between the two approaches is manifest. The first, by attempting to unravel the displacements which produced the structures found in the Jura will, if carried out correctly, restore the positions of the Jura/Molasse boundary to its original position before deformation. If this limit changes shape (e.g. twists) between the undeformed and deformed states,

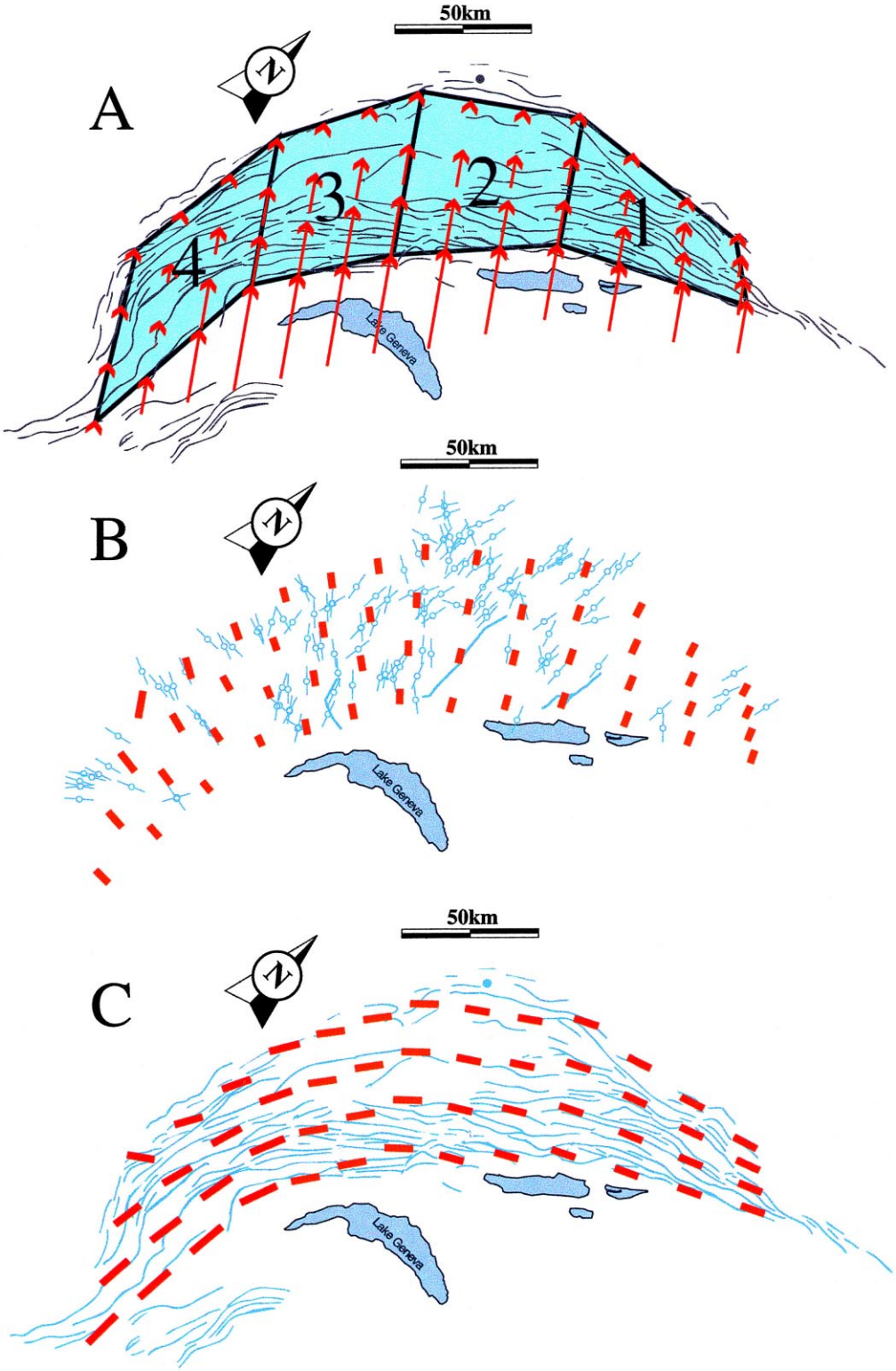

Fig. 5. Modelling the Jura using four quadrilateral domains. (a) The displacement field of Philippe (1995) is simplified to four points on the Jura/Molasse boundary, displaced differentially, in an identical direction. Jura/foreland boundary is fixed relative to these points. Four quadrilateral domains model the boundary conditions, and displacements (red vectors) are smoothly interpolated across them. Note that here, we pass from a reference element (rectangular) to two different deformed elements as outlined in the Appendix A. (b) Short axes calculated for the displacement field (red) compared to horizontal stylolites from the Jura (blue). (c) Long axes calculated for the displacement field (red) compared to fold axes from the Jura (blue).

the Molasse Basin must also have been internally deformed. The second approach attempts to find a model based upon analyses which are related to an instantaneous state of stress. As such, they ignore the large differential displacements along strike of the mountain belt accumulating over time. The arguments related to stress states are correct but do not take account of the dynamic evolution of the system over time.

We have adopted the results of Philippe (1995) and modified them slightly to model the total finite strain for the displacement field generated by two-dimensional plan view restoration of the Jura belt. Our model is simplified because rather than allowing a slight divergence of displacement vectors, we take only the displacements of four points along the Jura/Molasse boundary, and constrain them to be parallel (in an approximately northwest direction). We then pin the Jura/foreland boundary. Finally, as we model 'total' finite strain by such a technique, i.e. strain from displacement (in reality due to cumulative faulting and folding), we interpolate the displacements to decrease linearly to zero along the Jura/foreland boundary, from the values given along the Jura/Molasse boundary. These values are close to 30 km shortening (maximum) along the central and western Jura boundaries, but decline to zero at both the western and eastern Jura culminations. We substitute a continuous displacement function for what is in nature discontinuous and calculate a cumulative finite strain pattern for the Jura mountains, based on the sum of all displacement during their history. We compare the model strain data with observed strain features such as folds and horizontal stylolite peaks. The four points of known displacement are actually simulated by using quadrilateral domains as in the illustrative models.

Our results give directional information for short and long axes of the total finite strain ellipses predicted across the Jura. A rigidly parallel displacement field (Fig. 5a) produces a fanning strain pattern (Fig. 5) across a modelled Jura arc. Comparison with field data shows predicted short axes not fanning as strongly as stylolite teeth (Fig. 5b), with angular deviations of approximately 45° between measured and calculated values at the eastern and western terminations of the Jura. Predicted long axes orientations (Fig. 5c) match those of Jura folds across most of the eastern and central Jura with deviations of $< 10°$. Calculated strain axes swing by 73° in orientation across the model, which we may compare to the often-quoted 90° swing in orientation of the Jura structural grain along strike.

There are probable mechanical reasons for the difference in correspondence between the large, cumulative finite strains and different natural features. In the case of the stylolites, as already discussed (Fig. 3a), small deformations produce a widely fanning strain pattern, and since deformation is small, this would correspond closely to local principal stress trajectories. We also notice two contrasting orientations of stylolites in some places in the Jura. This has been interpreted as corresponding to two different regional stress fields. Other kinematic indicators (e.g. fault slickenslide analysis cf. Homberg et al. (1999)) also show these two trends. Such instantaneous measures of stress (or tiny strain) are not directly comparable to total finite strains. The fanning pattern is present for both model and natural data. However, deviations from transport direction are always lower in the case of the model where total shortening is large. The additional shortening component tends to pull strain axes closer into line with transport direction. Fold axes by contrast are far larger scale features and form over the course of the total deformation history of the mountain belt. The model is in very close correspondence with fold axes trends, since we compare the model to a quantity more representative of cumulative finite strain. This admittedly only offers a qualitative explanation, and the precise mechanics of the processes involved are far more complicated. Nevertheless, the likely overall geometry of total finite displacement in the Jura even when constrained to be rigorously parallel everywhere, produces the divergent pattern of strain we see in the Jura arc. It may be invoked as a mechanism for generating the arcuate geometry of the whole belt. There is no requirement of divergent transport along strike or secondary bending.

6. Conclusions

1. Illustrative models of transport parallel shear have shown any region inclined to transport direction undergoing constant displacement of one boundary will develop a fanning strain pattern, divergent from the transport direction.
2. If a region's width varies along strike and its boundary is moved a constant amount (even if the boundary is orthogonal to the transport direction) the shortening is consumed differentially along strike, generating a differential shear and again giving a fanning strain pattern, divergent from the transport direction. However, the degree of divergence for such a case is normally very small.
3. When a boundary of a region is displaced differentially along strike, the resulting fanning strain pattern is very clear, and shows strongest divergence from the transport direction along the line for which shortening in the model is a minimum. When shortening is zero along one line in such a model, the predicted strain axes along this line will diverge

by at least 45° from transport direction.

4. In general, these models illustrate that differential, parallel displacements of material in a region will generate fanning strain patterns.
5. A model of the Jura arc, allowing only parallel displacements and variable amounts of differential displacement and shortening along strike produces a fanning strain pattern across the width of the model region.
6. The orientations of stylolite teeth measured in the Jura (and also other kinematic indicators, e.g. fault slickenslides) show a similar fanning pattern but a stronger deviation from an assumed transport direction. Local angular differences of ca. 45° in orientation are found. Discrepancies most probably stem from modelling large, finite strains, and comparing them to features probably developed at a much earlier stage (lower strain) cf. point 3.
7. Fold axes trends, a measure of the 'structural grain' of the Jura arc, show a very close match to the orientations of modelled, long axes of finite strain ellipses (modelled variation along strike is 73°, change in trend of the Jura is ca. 90°). We attribute this to the fact that fold axes orientations develop over the entire deformation history of the belt, and consequently are closely related to the total calculated finite strains.
8. We conclude that geometrically constrained models of arcuate fold-and-thrust belt indentation give valuable information about the evolution of the indenter. Based on the evidence of several restorations (Laubscher, 1961; Philippe, 1995), the Molasse Basin has been deformed as it has a common boundary with the Jura arc, shown to have been rotated. Moreover, applying the finite displacements predicted by such a model generates a fanning strain pattern. Models of indentation based on stress patterns developing ahead of a rigid indenter (Laubscher, 1972; Homberg et al., 1999), predict fanning stress/strain patterns, but are instantaneous solutions to a problem. They ignore the accumulation of incremental strains over time and the changes in geometry of the system that this requires.

Acknowledgements

Very helpful reviews by David Ferrill and François Jouanne have substantially improved the scope of the manuscript. This study was supported by Swiss National Science Foundation Grants No. 20-43055.95 and 20-50535.97; it is a part of the PhD thesis of DH.

Appendix A. Mathematical derivations

Fig. A1 shows the general set up for the model. We see an initial rectangular element, $\mathbf{P}_n$ (n = 1–4), dimensions (L, W) transformed onto a general quadrilateral, $\mathbf{P}'_n$. The components of the vectors linking the two are named individually. These transformations give:

$$\mathbf{P_1} = \begin{pmatrix} 0 \\ 0 \end{pmatrix} \rightarrow \mathbf{P}'_1 = \begin{pmatrix} B \\ A \end{pmatrix},$$

$$\mathbf{P}_2 = \begin{pmatrix} L \\ 0 \end{pmatrix} \rightarrow \mathbf{P}'_2 = \begin{pmatrix} L+D \\ C \end{pmatrix},$$

$$\mathbf{P}_3 = \begin{pmatrix} L \\ W \end{pmatrix} \rightarrow \mathbf{P}'_3 = \begin{pmatrix} L+F \\ W+E \end{pmatrix},$$

$$\mathbf{P}_4 = \begin{pmatrix} 0 \\ W \end{pmatrix} \rightarrow \mathbf{P}'_4 = \begin{pmatrix} H \\ W+G \end{pmatrix}. \tag{A1}$$

We then derive four functions which individually attribute a value of 1 to one point $\mathbf{P}_n$ and simultaneously zero to all others (shape functions)

$$f_1 = (L - x_1)(W - x_2)\frac{1}{LW}$$

$$f_2 = x_1(W - x_2)\frac{1}{LW}$$

$$f_3 = x_1 x_2 \frac{1}{LW}$$

$$f_4 = (L - x_1)x_2\frac{1}{LW}. \tag{A2}$$

Now multiplying each function f_n by each new coordinate $\mathbf{P}'_n$ yields an equation of the form

$$\mathbf{x} = \sum_{n=1}^{4} f_n \mathbf{P}'_n, \tag{A3}$$

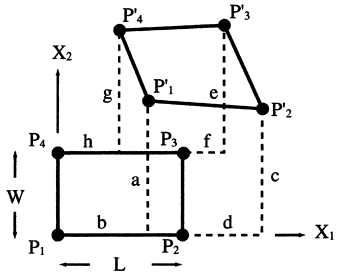

Fig. A1. Deriving transformation constants. The components a–h are shown positioned according to the equations derived in Appendix A. All models begin from a reference element with dimensions L, W as shown.

Where $\mathbf{x} = \begin{pmatrix} x_1 \\ x_2 \end{pmatrix}$ is the transformed co-ordinates of a point. The resulting displacement equations take a general form

$$x_1 = a_{11}X_1 + a_{12}X_2 + a_{13}X_1X_2 + a_{14}$$

$$x_2 = a_{21}X_1 + a_{22}X_2 + a_{23}X_1X_2 + a_{24}. \quad \text{(A4)}$$

We then differentiate with respect to X_1, and X_2 in turn. This gives us the deformation gradient matrix

$$\frac{\partial x_i}{\partial X_j} = \begin{bmatrix} a_{13}X_2 + a_{11} & a_{13}X_1 + a_{12} \\ a_{23}X_2 + a_{21} & a_{23}X_1 + a_{22} \end{bmatrix} = \mathbf{F}_{ij}. \quad \text{(A5)}$$

The matrix can be used in the manner $d\mathbf{x} = \mathbf{F} \cdot d\mathbf{X}$, thereby associating a vector at initial position $\mathbf{X}$ to another vector at final position $\mathbf{x}$. This specification (sometimes called Lagrangian) refers to the undeformed configuration. We find it more relevant to work in a deformed (Eulerian) configuration, since when making field measurements, we work in deformed material and ignore its initial position. We therefore prefer a specification $d\mathbf{X} = \mathbf{F}^{-1} \cdot d\mathbf{x}$, and require the inverse of the tensor $\mathbf{F}$. Various strain and deformation tensors exist and are well presented by (Malvern, 1969) (chapter 4). We use the Cauchy deformation tensor $\mathbf{B}^{-1}$. This gives the initial squared length (dS^2) of an element $d\mathbf{x}$ identified in the deformed configuration

$$\mathbf{B}^{-1} = (\mathbf{F}^{-1})^t \cdot \mathbf{F}^{-1}. \quad \text{(A6)}$$

So, we have the general displacement equation for the rectangle onto any quadrilateral. If we wish to take a general quadrilateral as the **initial** shape and deform that, a solution is also possible. We work from an initial rectangular element—a reference element.

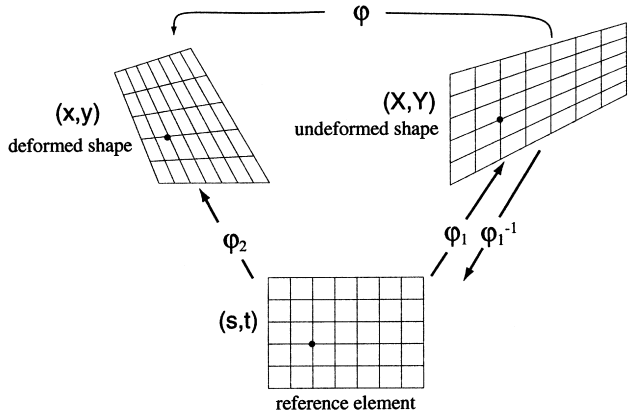

Fig. A2. Although we want a single function φ, it is easier to work from a reference element and carry out two separate transformations. We therefore work between three separate co-ordinate systems, (s, t), (X, Y), (x, y) defining the original co-ordinate grid in (s, t). Functions mentioned in the text are shown schematically.

Eqns (A4) govern the transformation of the rectangle onto **both** any initial quadrilateral and any final quadrilateral. Thus a co-ordinate point (s, t) in the reference element (Fig. A2) is associated to a point (X, Y) in the initial configuration by application φ_1 and to a point (x, y) in the final configuration by application φ_2. Both applications φ_1 and φ_2 are of the form of Eqns (A4). A global application φ can be imagined which directly associates a point (X, Y) to a point (x, y). It is equivalent to the composite function

$$\varphi_2\left(\varphi_1^{-1}(X,Y)\right) \text{ or } \varphi_2 \cdot \varphi_1. \quad \text{(A7)}$$

It is also equivalent to associating either 'end' of the equations

$$\varphi_1(s,t) = (X,Y) \text{ and } \varphi_2(s,t) = (x,y). \quad \text{(A8)}$$

By using (s, t) this way, we can effect a co-ordinate transformation of a known point in ALL co-ordinate systems, without directly knowing φ_1^{-1}. To calculate deformations, we need to know $\mathbf{D}\varphi$.

$$\mathbf{D}\varphi = \mathbf{D}\left(\varphi_2 \cdot \varphi_1^{-1}\right) = \mathbf{D}\varphi_2 \cdot \mathbf{D}\left(\varphi_1^{-1}\right) = \mathbf{D}\varphi_2 \cdot \mathbf{D}\varphi_1^{-1}. \quad \text{(A9)}$$

We need to find $\mathbf{D}\varphi^{-1}$.

$$\mathbf{D}\varphi^{-1} = \left(\mathbf{D}\varphi_2 \cdot \mathbf{D}\varphi_1^{-1}\right)^{-1} = \mathbf{D}\varphi_1 \cdot \mathbf{D}\varphi_2^{-1}. \quad \text{(A10)}$$

Then, like Eqns (A6)

$$\mathbf{B}^{-1} = \left(\mathbf{D}\varphi^{-1}\right)^t \cdot \mathbf{D}\varphi^{-1} = \left(\mathbf{D}\varphi_2^{-1}\right)^t \cdot \mathbf{D}\varphi_1^t \cdot \mathbf{D}\varphi_1^t \cdot \mathbf{D}\varphi_2^{-1}. \quad \text{(A11)}$$

References

Argand, E., 1922. La tectonique de l'Asie. In: Congrès Géologique International. Extrait du compte-rendu du XIIIe congrès géologique internationale, Brussels, pp. 171–372.

Aubert, D., 1945. Le Jura et la tectonique d'écoulement. Memoire de la Société Vaudoise des Sciences Naturelles 12, 93–152.

Burkhard, M., 1990. Aspects of the large scale Miocene deformation in the most external part of the Swiss Alps (Subalpine Molasse to the Jura fold belt). Eclogae Geologicae Helvetiae 83, 559–583.

Burkhard, M., Sommaruga, A., 1998. Evolution of the Western Swiss Molasse Basin structural relations with the Alps and the Jura belt. In: Mascle, A., Puigdefabregas, C., Luterbacher, H.P., Fernandez, M. (Eds.), Cenozoic Foreland Basins of Western Europe (134). Geological Society Special Publications, London, pp. 279–298.

Buxtorf, A., 1916. Prognosen und Befunde beim Hauensteinbasis und Grenchenberg tunnel und die Bedeutung der letzteren für die Geologie der Juragebirges. Verh. Naturforsch. Ges. Basel 27, 185–254.

Carey, S.W., 1955. The orocline concept in geotectonics. Proceedings of the Royal Society of Tasmania. 89, 255–288.

Debrand Passard, S., Courbouleix, S., Leinhardt, M.-J., 1984.

Synthèse géologique du Sud–Est de la France. Stratigraphie et Paléogéographie, Orléans.
Ferrill, D.A., Groshong, R.H., 1993. Kinematic model for the curvature of the northern Subalpine Chain, France. Journal of Structural Geology 15, 523–541.
Hindle, D., Burkhard, M., 1999. Strain, displacement and rotation associated with the formation of curvature in fold belts; the example of the Jura arc. Journal of Structural Geology 21, 1089–1101.
Homberg, C., Lacombe, O., Angelier, J., Bergerat, F., 1999. New constraints for indentation mechanisms in arcuate belts from the Jura Mountains, France. Geology 27, 827–830.
Howard, J.H., 1968. The use of transformation constants in finite homogeneous strain analysis. American Journal of Science 266, 497–506.
Laubscher, H.P., 1961. Die Fernschubhypothese der Jurafaltung. Eclogae Geologicae Helvetiae 54, 221–282.
Laubscher, H.P., 1972. Some overall aspects of Jura dynamics. American Journal of Science 272, 293–304.
Malvern, L.E., 1969. Introduction to the Mechanics of a Continuous Medium. Prentice-Hall, Englewood Cliffs, NJ.
Marshak, S., 1988. Kinematics of orocline and arc formation in thin-skinned orogens. Tectonics 7, 73–86.
Means, W.D., 1976. Stress and Strain; Basic Concepts of Continuum Mechanics for Geologists. Springer-Verlag, New York.
Molnar, P., 1983. Average regional strain due to slip on numerous faults of different orientations. Journal of Geophysical Research 88, 6430–6432.
Pavoni, N., 1961. Faltung durch Horizontalvershiebung. Eclogae Geologicae Helvetiae 54, 515–534.
Philippe, Y., 1994. Transfer zone in the Southern Jura Thrust Belt (eastern France) Geometry, development and comparison with analogue modelling experiments. In: Mascle, A. (Ed.), Hydrocarbon and Petroleum Geology of France (special issue). European Association of Petroleum Geology, pp. 327–346.
Philippe, Y. 1995. Rampes latérales et zones de transfert dans les chaines plissées. Unpublished PhD thesis, Université de Savoie.
Ramsay, J.G., 1976. Displacement and strain. In: by London, R.S.O. (Ed.), A Discussion on Natural Strain and Geological Structure. Royal Society of London, London, pp. 3–25.
Reches, Z., 1978. Analysis of faulting in three-dimensional strain field. Tectonophysics 47, 109–129.
Ries, A.C., Shackleton, R.M., 1976. Patterns of strain variations in arcuate fold belts. Philosophical Transactions of the Royal Society of London A 283, 281–288.
Sanderson, D.J., Marchini, W.R.D., 1984. Transpression. Journal of Structural Geology 6, 449–458.
Schardt, H., 1906. deux coupes générales à travers la chaîne du Jura. Archives des Sciences Physiques et Naturelles, Genève XXIII.
Schardt, H., 1908. Les causes du plissement et des chevauchements dans le Jura. Eclogae Geologicae Helvetiae X, 484–488.
Sommaruga, A., 1995. Tectonics of the Central Jura, and the Molasse Basin. New insights from the interpretation of seismic reflection data. Bulletin de la Société Neuchâteloise des Sciences Naturelles 118, 95–108.
Sommaruga, A., 1996. Geology of the central Jura and the Molasse Basin: new insight into an evaporite-based foreland fold and thrust belt. Unpublished PhD thesis, Neuchâtel.
Sommaruga, A., 1999. Décollement tectonics in the Jura foreland fold-and-thrust belt. Marine and Petroleum Geology 16, 111–134.
Ziegler, P.A., 1982. Geological Atlas of Western and Central Europe. Shell International Petroleum, Maatshappij, BV.